MODELING AND OPTIMIZATION RESEARCH FOR DYNAMIC TRANSMISSION PROCESS OF BALISE TELE-POWERING SIGNAL IN HIGH-SPEED RAILWAYS

Lin-Hai Zhao[*] and Ying Jiang

School of Electronics and Information Engineering, Beijing Jiaotong University, Beijing 100044, China

Abstract—As key components of the train control system, balise and Balise Transmission Module (BTM) cooperate with each other and fulfill the ground-train information transmission to ensure the safety and reliability of train operation. Aiming at the requirements for future developments of high-speed railway, this paper builds the model for the dynamic transmission process of the balise tele-powering signal using finite element method and electromagnetic field theory, respectively. The paper analyzes the change law of the magnetic flux density distribution within the balise receiving antenna, and derives expressions for the balise induced voltage amplitude envelope based on train speed. Then, the paper carries out the performance optimization to the existing balise system from two perspectives of the balise mounting style and the BTM mounting height. Experiments show that the proposed optimization measures can substantially enhance the system's adaptability to the ever-increasing train operation speed from the existing 448 km/h to 523 km/h. Furthermore, a potential optimization scheme with respect to the BTM mounting angle which enables huge promotion of the system performance is also discussed and proposed.

1. INTRODUCTION

With the rapid development of China's railway system in recent years, train running speed is increasing even faster. For example, China's CRH-380A train broke the world record for unmodified commercial use with a speed of 486.1 km/h during trial service on the Beijing-Shanghai high-speed railway [1], while its operation speed in practical

application stage stays around 300 km/h [2]. In Europe, Japan and other countries, the maximum operation speeds of their high-speed railways are about 250 km/h [3]. The high-speed operation of train has demanded even higher requirements for the corresponding train control system, e.g., CTCS (Chinese Train Control System), ETCS (European Train Control System) [4]. As shown in Figure 1, composed of on-board Balise Transmission Module (BTM) and ground balise, the balise information transmission system (BITS) is a kind of high-rate point-mode data transmission equipment and serves as an important part of the train control system. The system function of BITS is accomplished by two signal transmission processes, i.e., the tele-powering transmission process where the BTM radiates energy waves to activate the ground balise to start to work and the up-link signal transmission process where the ground balise transmits important control information to the train subsequently. Through the two processes, the ground-train point-mode information transmission is achieved, and the telegram information including geographical position, route data and temporary speed limit is passed to the Vital Computer (VC) [5], which continuously calculates the dynamic speed profile from these data and other information concerning locomotive performances, thus realizing the real-time supervision of train speed. Therefore, the information transmission process of BITS is very important for train operation safety.
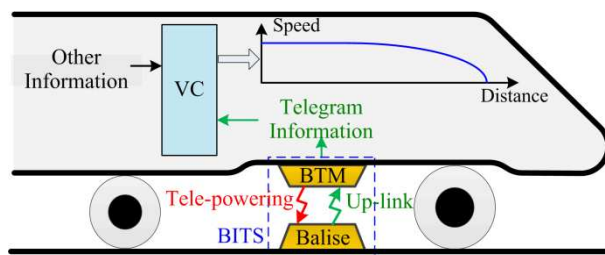
Figure 1. Function schematic of the BITS in train control system.

Currently, researches regarding the BITS are mainly focused on up-link signal demodulation, testing and performance assessment, transmission reliability, balise placement, etc. In [6], the coding and decoding method of BITS is researched and verified in theory that the safety of balise information transmission is assured. An up-link signal detection method based on continuous wavelet transform was proposed in [7]. With respect to BTM testing and evaluation, some

crucial techniques of the on-board testing equipment were investigated using radio frequency theory, spectrum analysis and virtual instrument methods [8]. In [9], a testing program was designed to evaluate the basic performance and characteristics of the BTM. As for transmission reliability, the crosstalk problem encountered with major trackside equipment such as the Balise and the Loops was analyzed in [10]. The reliability of the on-board BTM was analyzed in terms of the number of balise passages with error free telegram delivery [11]. Given the importance of balices in train detection, a colored Petri net model of the discrete point positioning system was proposed to analyze the impact of dysfunctions in train detection system [12]. In [13], the Genetic Algorithm and Kalman filtering concept were used to find the optimum places of balices. In [14], the balise up-link data transmission process was modeled using finite element method and the characteristics including the spectrum and the time-frequency distribution of the up-link signal was analyzed.

From the above description we can see that few researches have been devoted to the ground-train balise information transmission process so far except for [14]. However, considering the future developments of railway, whether the BITS devices in use can adapt to the further increase of train operation speed has become a practical issue and drawn much attention already. Therefore, it is necessary to carry out optimization measures to the existing system to promote its performance and meet the requirements of train speed increase. From this point of view, the research that's only related to the up-link signal transmission at present is not sufficient and needs to be perfected. This paper aims to study the dynamic transmission process of the balise tele-powering signal in basic theoretical level, and then implement the optimization for BITS by combining the two transmission processes together.

The remainder of this paper is organized as follows: Section 2 introduces the modeling and simulation analysis of the dynamic transmission process of the balise tele-powering signal based on finite element method (FEM) and electromagnetic field theory. Section 3 describes the performance optimization to the existing system from views of the balise mounting style and the BTM mounting height (BMH), and proposes corresponding optimization measures. Section 4 presents the experimental verification for the proposed optimization measures. Section 5 discusses and proposes a potential optimization scheme regarding the pitch angle of the BTM transmitting antenna. Finally, Section 6 concludes the paper.

2. MODELING AND SIMULATION OF THE DYNAMIC TRANSMISSION PROCESS OF BALISE TELE-POWERING SIGNAL

2.1. Basic Structure and Working Principle of BITS

Figure 2 shows the basic structure and working principle of the BITS. Usually, the on-board BTM continuously radiates tele-powering signal generated in the corresponding module via the BTM transmitting antenna, whereas the ground balise remains dormant until the train passes by. When a train comes close to the balise, through electromagnetic induction [15], the induced voltage [16] forms in the balise receiving antenna, and as the train approaches, it gradually gets stronger, and finally reaches the given threshold to activate the balise, making it transform from dormant state to operation state. Then, in the telegram signal generation module, the telegram data stored is modulated as the up-link signal and transmitted via the balise transmitting antenna with given rate. Meanwhile, the up-link signal is induced in the BTM receiving antenna and sent to the telegram signal processing module to be filtered, demodulated and decoded, then the contained information is extracted and provided to the VC for train speed control. As the train continues to travel, the balise induced voltage gradually decreases and falls below the threshold at last, and the balise gets into dormancy again.

(a) (b)
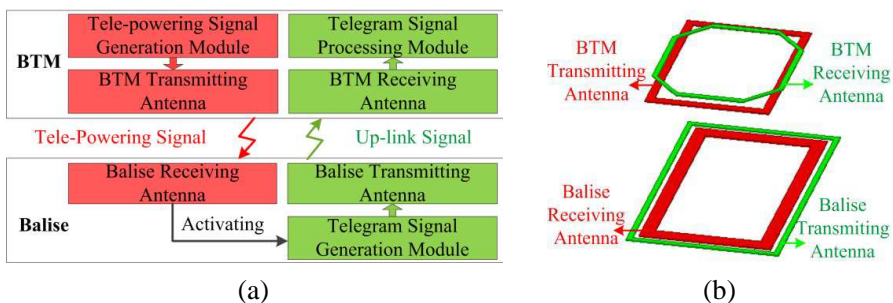
Figure 2. Basic structure and working principle of the BITS. (a) Structure of the BITS. (b) Shape and architecture of the coil antennas of the BTM and the balise.

2.2. Modeling and Simulation of the BITS Based on FEM

A precise model is needed for the physical simulation to incorporate the essential dynamics of the information transmission process of

BITS [17–19], and the FEM that provides accurate numerical approximations can be one of the best choices [20–22]. In this paper, the 3D-FEM [23] has been used to investigate the magnetic field distribution and the voltage induced in the balise receiving antenna, as shown in Figure 3.
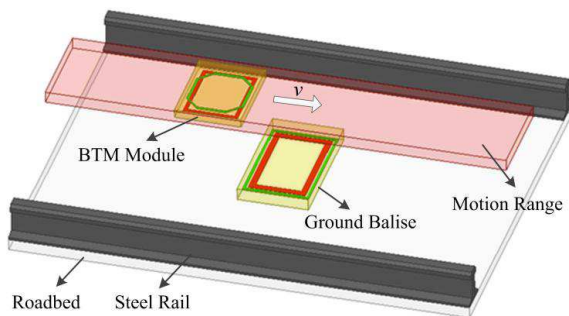
Figure 3. Model of the BITS based on FEM.

The FEM based model mainly consists of the BTM module, balise, steel rails, and roadbed, and the associated electromagnetic parameters are listed in Table 1.

Table 1. List of the electromagnetic parameters of the materials used.

Object	μ_r	ε_r	σ (S/m)
Coil Antenna	1	0.999991	58000000
Steel Rail	80	300	4760000
Roadbed	4.8	1	0

Since the accuracy requirements of the coil antennas are relatively high, the meshes applied to them are very dense, while the meshes applied to the steel rails and the roadbed are a little sparse, as shown in Figure 4.

We set the BTM module to be right above the balise and start the transient electromagnetic simulation of the complete FEM based model. The simulation conditions are set as follows: BTM translation speed $v = 300$ km/h, operating frequencies of the tele-powering signal, up-link signal, and the signal flowing through the steel rails are $f_{ct} = 27.095$ MHz, $f_{cu} = 4.234$ MHz, and $f_{cr} = 2600$ Hz, respectively. The magnetic field distribution (MFD) [24] of the longitudinal section plane of the BITS and the induced voltage of the balise receiving antenna are shown in Figures 5(a) and 5(b).
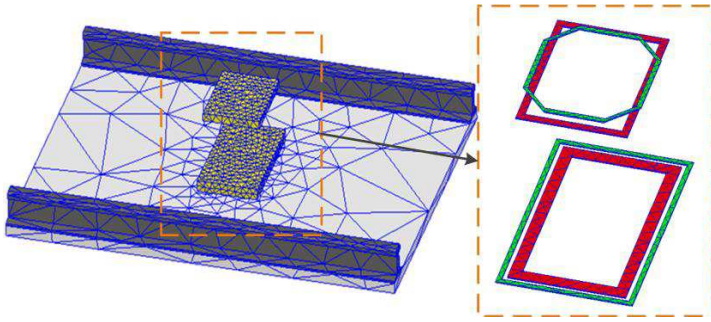
Figure 4. Meshing of the FEM based model.
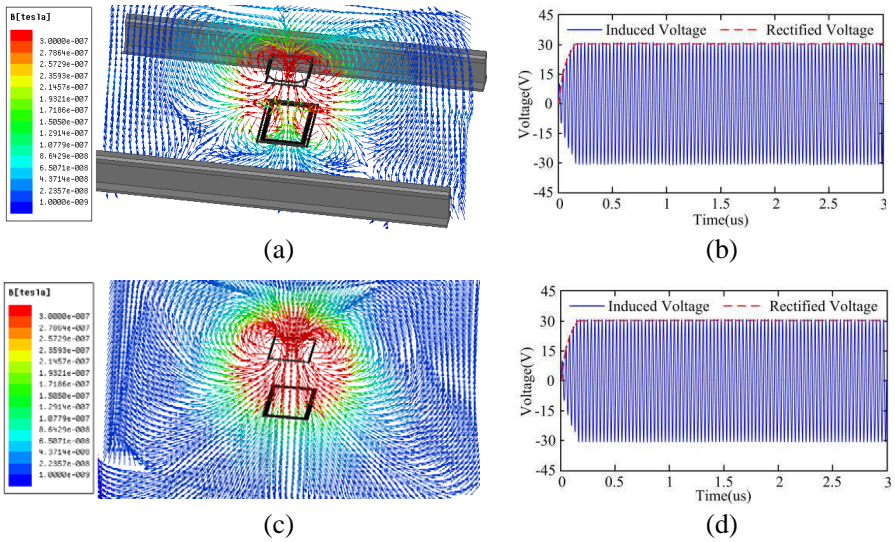
Figure 5. Simulation results of the MFD and the balise induced voltage. Figures (a) and (b) correspond to the complete model. Figures (c) and (d) correspond to the simplified model.

Figure 5(a) shows that because the BTM is very close to the balise and both the tele-powering and up-link transmitting antennas are in operation state, the magnetic field between the BTM and the balise is very strong, whereas the magnetic field in the ambient space far from the antennas is very weak. In Figure 5(b), the solid line represents the induced voltage of the balise receiving antenna, which is then rectified by the bridge rectifier and filtered by the capacitors to become the signal represented by the dashed line.

Since the signal frequency of this transmission process is relatively high and the solution domain relatively big, the number of meshes may be pretty large to reach sufficient accuracies. In a PC with the CPU of 3.4 GHz and memory of 4 GB, the time required for the above transient simulation is about 4 hours, if we simulate the complete transmission process when the BTM passes by the balise, the required time and memory may substantially increase and even cause the software to stop calculating. Thus, it is necessary to simplify the FEM model to reduce the simulation time with the premise that the sufficient accuracy is guaranteed. Hence, we take out the steel rails and the antennas of the up-link transmission to get the simplified model which is just composed of the BTM transmitting antenna and the balise receiving antenna, and the corresponding simulation results are shown in Figures 5(c) and 5(d). Careful contrast of Figures 5(a) and 5(c) shows that the magnetic field distributions of the complete model and the simplified model generally agree with each other, and a little difference is discerned in the vicinity of the balise due to the influences of the up-link signal and the signal that flows through the steel rails. What's more important is in Figure 5(b) and 5(d), where we find that the simulation results of the balise induced voltage are almost the same, mainly because the frequency bands of tele-powering signal and other two signals are quite different. Therefore, the simplified FEM model is feasible.

2.3. Modeling and Simulation of the Dynamic Transmission Process of Balise Tele-powering Signal Using Electromagnetic Field Theory

Figure 6 shows the simplified model. We take the center of the ground balise O as the origin of a Cartesian coordinate system and directions parallel to the EF and FG sides of the balise receiving antenna (hereafter called the balise antenna because only the tele-powering transmission is dealt with) as the OX and OY axes, respectively.

The dimensions of the balise antenna and BTM transmitting antenna (hereafter called the BTM antenna) are $EF = GH = 2l_c$, $FG = HE = 2l_d$, and $AB = CD = 2l_a$, $BC = DA = 2l_b$, respectively. The coordinate of the center of the BTM antenna O_1 is $(x', 0, h)$, the vertical distance from O_1 to the balise antenna is h, and without loss of generality, the pitch angle of the BTM antenna is assumed as α. Plane $AB'C'D$ is parallel with the XOY plane, and points B' and C' are the projections of B and C in XOY plane, respectively. Here we suppose the BTM antenna translates in $+x$ direction with the velocity of v, and
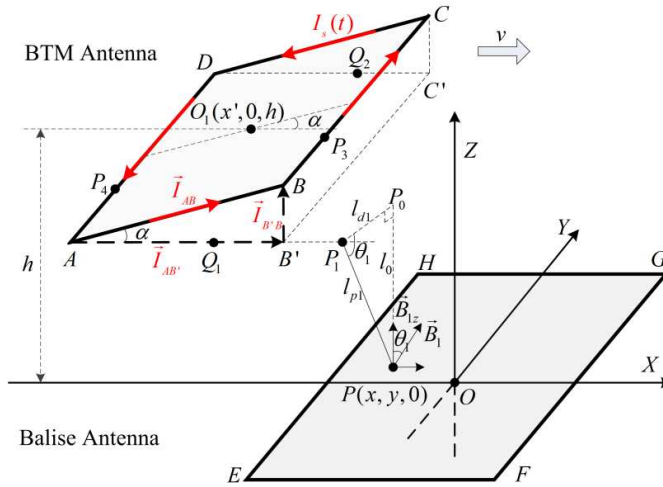
Figure 6. Modeling of the dynamic transmission process of the balise tele-powering signal.

the current flowing through the BTM antenna, $I_s(t)$, is represented by

$$I_s(t) = A_s \cos(2\pi f_c t + \phi_0) \tag{1}$$

where A_s, f_c, and ϕ_0 are the amplitude, signal frequency and initial phase, respectively.

First we calculate the z-axis component of the MFD generated by side AB, i.e., $B_{1z}(x', t, \alpha)$. As shown in Figure 6, we resolve the current on side AB, $\vec{I}_{AB}$, into $\vec{I}_{AB'} + \vec{I}_{B'B}$, according to Ampere circuital law [25], the MFD generated by current $\vec{I}_{B'B}$ is parallel with the XOY plane and does not contribute to $B_{1z}(x', t, \alpha)$, thus $B_{1z}(x', t, \alpha)$ is equivalent to the z-axis component of the MFD generated by side AB'. Let P_0 be the projection of P on plane $AB'C'D$, P_1 be the foot of a perpendicular from P to line AB'. Suppose $PP_0 = l_0$, $P_0P_1 = l_{d1}$, $PP_1 = l_{p1}$, $\theta_1 = \angle P_0P_1P$, and x_{q1} is the x coordinate of a random point Q_1 on side AB', then we have

$$l_0 = h - l_a \sin \alpha, \quad l_{d1} = l_b + y, \quad l_{p1} = \sqrt{l_{d1}^2 + l_0^2}, \quad \cos \theta_1 = l_{d1}/l_{p1} \tag{2}$$

Supposing that μ_0 is the permeability in vacuum, the Biot-Savart law [26] gives the MFD $B_1(x', t, \alpha)$ generated by side AB' as

$$B_1(x', t, \alpha) = \frac{\mu_0 I_s(t)}{4\pi} \int_{x'-l_a \cos \alpha}^{x'+l_a \cos \alpha} l_{p1} \cdot \left(\sqrt{(x_{q1} - x)^2 + l_{p1}^2} \right)^{-3} dx_{q1} \tag{3}$$

The angle between $B_1(x', t, \alpha)$ and z-axis is θ_1, so we perform resolution to $B_1(x', t, \alpha)$ and its z-axis component, i.e., $B_{1z}(x', t, \alpha)$ is obtained as

$$B_{1z}(x', t, \alpha) = B_1(x', t, \alpha) \cos \theta_1$$

$$= \frac{\mu_0 I_s(t)}{4\pi} \int_{x'-l_a \cos \alpha}^{x'+l_a \cos \alpha} l_{d1} \cdot \left(\sqrt{(x_{q1}-x)^2 + l_{p1}^2} \right)^{-3} dx_{q1} \quad (4)$$

For side CD, the solving method for MFD is similar to that of side AB. Hence, the z-axis component of the MFD generated by side CD, $B_{2z}(x', t, \alpha)$ is given by

$$B_{2z}(x', t, \alpha) = \frac{\mu_0 I_s(t)}{4\pi} \int_{x'-l_a \cos \alpha}^{x'+l_a \cos \alpha} l_{d2} \cdot \left(\sqrt{(x_{q2}-x)^2 + l_{p2}^2} \right)^{-3} dx_{q2} \quad (5)$$

where $l_{d2} = l_b - y$, $l_{p2} = \sqrt{l_{d2}^2 + l_0^2}$, and x_{q2} is the x-coordinate of the random point Q_2 on side DC'.

For side BC and DA, let $P_3(x_3, y_3, z_3)$ and $P_4(x_4, y_4, z_4)$ be the feet of perpendiculars from P to sides BC and DA, respectively, and y_{q3} and y_{q4} the y coordinates of the arbitrary points on both sides. Suppose $PP_3 = l_{p3}$, $PP_4 = l_{p4}$, and it yields

$$\begin{aligned} x_3 = x' + l_a \cos \alpha, \quad z_3 = h + l_a \sin \alpha, \quad l_{p3} = \sqrt{(x-x_3)^2 + z_3^2} \\ x_4 = x' - l_a \cos \alpha, \quad z_4 = h - l_a \sin \alpha, \quad l_{p4} = \sqrt{(x-x_4)^2 + z_4^2} \end{aligned} \quad (6)$$

Then the MFD $B_3(x', t, \alpha)$ and $B_4(x', t, \alpha)$ generated by side BC and DA can be expressed as

$$\begin{aligned} B_3(x', t, \alpha) = \frac{\mu_0 I_s(t)}{4\pi} \int_{-l_b}^{l_b} l_{p3} \cdot \left(\sqrt{(y_{q3} - y)^2 + l_{p3}^2} \right)^{-3} dy_{q3} \\ B_4(x', t, \alpha) = \frac{\mu_0 I_s(t)}{4\pi} \int_{-l_b}^{l_b} l_{p4} \cdot \left(\sqrt{(y_{q4} - y)^2 + l_{p4}^2} \right)^{-3} dy_{q4} \end{aligned} \quad (7)$$

In order to resolve and acquire the z-axis components of $B_3(x', t, \alpha)$ and $B_4(x', t, \alpha)$, we project Figure 6 into the XOZ plane as shown in Figure 7. Side DA and BC are projected to point A_1 and B_1, respectively, both side AB and CD are projected to line A_1B_1, the balise antenna is projected to line E_1F_1, P is projected to $P'(x, 0)$ and the projection of P' on side A_1B_1 is P_0'. The BTM center $O_1(x', h)$ remains unchanged, and O_1K is a half line parallel with the OX axis.

Suppose the angle that O_1P' makes with O_1K is γ, the angle between B_1P' and A_1B_1 is θ_3, and the angle between A_1P' and A_1B_1
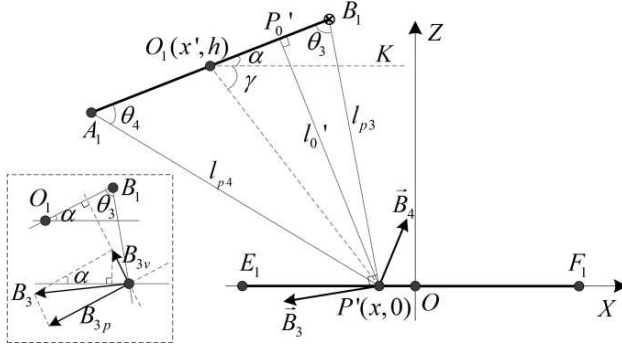
Figure 7. Projection of Figure 6 into the XOZ plane.

is θ_4, $P'P_0' = l_0'$, and it arrives

$$\gamma = \begin{cases} \arctan(h/(x-x')), & x-x' > 0 \\ \pi + \arctan(h/(x-x')), & x-x' < 0 \\ \pi/2, & x-x' = 0 \end{cases} \quad (8)$$

$$\begin{cases} l_0' = (h + (x-x')\tan\alpha)\cos\alpha \\ \cos\theta_3 = B_1P_0'/B_1P' = (l_a - l_0'\cot(\gamma+\alpha))/l_{p3}, & \sin\theta_3 = l_0'/l_{p3} \\ \cos\theta_4 = A_1P_0'/A_1P' = (l_a + l_0'\cot(\gamma+\alpha))/l_{p4}, & \sin\theta_4 = l_0'/l_{p4} \end{cases} \quad (9)$$

The resolution process of $B_3(x', t, \alpha)$ is shown in the left lower dashed frame in Figure 7, where B_{3p} and B_{3v} refer to the two components of $B_3(x', t, \alpha)$ whose directions are parallel and vertical with line O_1B_1, respectively, and satisfy $B_{3p} = B_3\cos\theta_3$, $B_{3v} = B_3\sin\theta_3$. In addition, we perform resolutions to B_{3p} and B_{3v} to obtain their z-axis components, thus, the z-axis component of $B_3(x', t, \alpha)$, $B_{3z}(x', t, \alpha)$, is obtained as

$$B_{3z}(x', t, \alpha) = B_3(x', t, \alpha) \cdot (\cos\theta_3\cos\alpha - \sin\theta_3\sin\alpha) \quad (10)$$

This resolution method also holds for $B_4(x', t, \alpha)$, whose z-axis component is given by

$$B_{4z}(x', t, \alpha) = B_4(x', t, \alpha) \cdot (\cos\theta_4\cos\alpha + \sin\theta_4\sin\alpha) \quad (11)$$

To sum up, the total MFD $B_z(x', t, \alpha)$ is

$$B_z(x', t, \alpha) = B_{1z}(x', t, \alpha) + B_{2z}(x', t, \alpha) + B_{3z}(x', t, \alpha) + B_{4z}(x', t, \alpha) \quad (12)$$

However, in practical situation, the BTM antenna is usually mounted horizontally, i.e., $\alpha = 0$ while the BMH h remains unchanged.

Substitute $\alpha = 0$ into Eqs. (2)–(12), and let

$$N_{fs}(l_a, l_b, h, x', x, y)$$

$$= \frac{\mu_0}{4\pi} \begin{Bmatrix} (l_b + y) \cdot \int_{x'-l_a}^{x'+l_a} \left(\sqrt{(x_{q1} - x)^2 + (l_b + y)^2 + h^2} \right)^{-3} dx_{q1} \\ + (l_b - y) \cdot \int_{x'-l_a}^{x'+l_a} \left(\sqrt{(x_{q2} - x)^2 + (l_b - y)^2 + h^2} \right)^{-3} dx_{q2} \\ + \int_{-l_b}^{l_b} \left(\sqrt{(y_{q3} - y)^2 + (x - (x' + l_a))^2 + h^2} \right)^{-3} dy_{q3} \\ \cdot ((l_a - (x - x')) \cos \alpha - h \sin \alpha) \\ + \int_{-l_b}^{l_b} \left(\sqrt{(y_{q4} - y)^2 + (x - (x' - l_a))^2 + h^2} \right)^{-3} dy_{q4} \\ \cdot ((l_a + (x - x')) \cos \alpha + h \sin \alpha) \end{Bmatrix} \quad (13)$$

Then the z-axis component of the MFD at an arbitrary point $P(x, y, 0)$ generated by the horizontally mounted BTM antenna, $B_z(x', t)$, is expressed as

$$B_z(x', t) = I_s(t) \cdot N_{fs}(l_a, l_b, h, x', x, y) \quad (14)$$

Thereby, the magnetic flux $\psi(x', t)$ through the balise antenna is given by

$$\psi(x', t) = \int_{-l_c}^{l_c} \int_{-l_d}^{l_d} B_z(x', t) dx dy$$

$$= I_s(t) \cdot \int_{-l_c}^{l_c} \int_{-l_d}^{l_d} N_{fs}(l_a, l_b, h, x', x, y) dx dy \quad (15)$$

In Equation (15), because l_a, l_b, l_c, and l_d are constants, the result of the integral term is only related to h and x', and can be represented by

$$\varphi(h, x') = \int_{-l_c}^{l_c} \int_{-l_d}^{l_d} N_{fs}(l_a, l_b, h, x', x, y) dx dy \quad (16)$$

Then Equation (15) becomes

$$\psi(x', t) = I_s(t) \cdot \varphi(h, x') \quad (17)$$

According to Faraday's law of electromagnetic induction [27], the electromotive force (EMF) of the balise antenna loop $\varepsilon(x', t)$ equals the induced EMF $\varepsilon_{in}(x', t)$ caused by the time-variant current plus the motional EMF $\varepsilon_{mo}(x', t)$ caused by the translation of the balise antenna, i.e.,

$$\varepsilon(x', t) = \varepsilon_{in}(x', t) + \varepsilon_{mo}(x', t) \quad (18)$$

where the induced EMF is expressed as

$$\varepsilon_{in}(x', t) = -d\psi(x', t)/dt = -\varphi(h, x') \cdot dI_s(t)/dt$$
$$= 2\pi f_c A_s \varphi(h, x') \sin(2\pi f_c t + \phi_0) \quad (19)$$

As to the motional EMF, since only two sides HE and GF cut the magnetic induction line, and it can be represented by the difference of the separate EMF caused by the two sides, i.e.,

$$\varepsilon_{mo}(x',t) = B_{HE}l_{HE}v - B_{GF}l_{GF}v = 2l_d v \left(B_{HE}(x',t) - B_{GF}(x',t)\right) \quad (20)$$

Hence, the induced voltage of the balise antenna coil is expressed as

$$U_{ev}(x',t) = q \cdot \varepsilon(x',t) = q \cdot \varepsilon_{in}(x',t) + q \cdot \varepsilon_{mo}(x',t) \quad (21)$$

where q is the quality factor [28, 29] of the balise antenna loop.

According to balise mounting and application specification [30, 31] and on-site investigations, the simulation conditions are set as follows: $2l_a = 220\,\text{mm}$, $2l_b = 295\,\text{mm}$, $2l_c = 200\,\text{mm}$, $2l_d = 390\,\text{mm}$, $h = 0.33\,\text{m}$, $A_s = 0.72\,\text{A}$, $f_c = 27.095\,\text{MHz}$, $\phi_0 = 0$, and $q = 12$.

Let the location of the BTM center be $x' = -0.7\,\text{m}$, $-0.45\,\text{m}$, $-0.2\,\text{m}$, 0, 0.2 m, 0.45 m, 0.7 m, respectively. By means of quasistatic approximation and set the current flowing through the BTM antenna to be the maximum, i.e., A_s, we simulate the MFD distribution within the balise antenna according to Equation (14) when the train passes by the balise in $+x$ direction, as shown in Figure 8.

Figure 8(a) shows that when $x' = -0.7\,\text{m}$, the amplitude of the MFD within the balise antenna is fairly low, and the order of magnitude is only 10^{-9}. Figure 8(b) shows that when $x' = -0.45\,\text{m}$, the amplitude of the MFD has reached the minimum (called the zero-value area) as manifested by the light-colored stripe in the middle of the balise antenna. It indicates that in the range $x' < -0.45\,\text{m}$, the amplitude of the MFD is not just increasing all along but increasing first, and
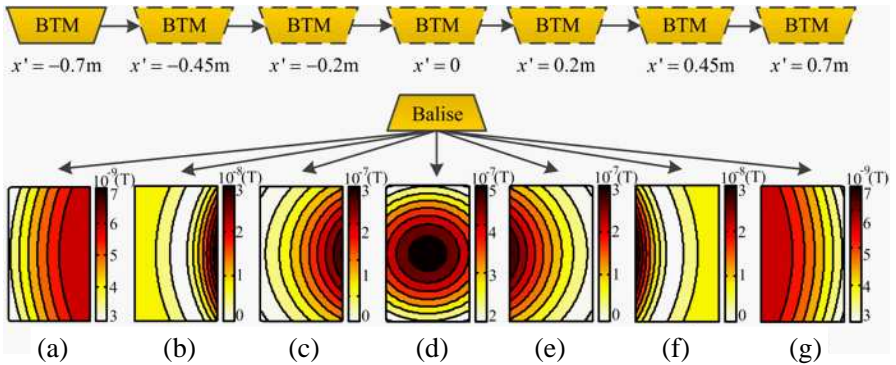
Figure 8. MFD distributions within the balise antenna at different BTM locations (each figure is flipped horizontally for better display of the change law of the MFD).

then decreasing to the minimum. As the BTM antenna continues to translate, the amplitude of the MFD increases again as shown in Figure 8(c), and reaches the maximum with the order of magnitude up to 10^{-7} at $x' = 0$ where the BTM antenna is just above the balise antenna as shown in Figure 8(d). When the BTM antenna has been translated to the positive half of the x-axis as shown in Figures 8(e)–8(g), the change law of the MFD is similar to that of the negative half of x-axis.

Figure 8 discloses that the maximum values of $B_{HE}(x', t)$ and $B_{GF}(x', t)$ are about 5×10^{-7} (T), so $|B_{HE}(x', t) - B_{GF}(x', t)| < 5 \times 10^{-7}$ (T). In practical conditions, $v < 200$ m/s, hence

$$q \cdot \varepsilon_{mo}(x', t) < 12 \times 0.39 \times 200 \times 5 \times 10^{-7} = 4.7 \times 10^{-4} \text{ (V)} \quad (22)$$

The induced voltage of motional EMF is so little compared to the threshold of the balise start-up voltage which is $V_{th} = 3.3$ V, and can be omitted. Therefore, the total induced voltage of the balise antenna coil satisfies

$$U_{ev}(x', t) = q \cdot \varepsilon_{in}(x', t) = 2\pi f_c A_s q \cdot \varphi(h, x') \sin(2\pi f_c t + \phi_0) \quad (23)$$

Here we define

$$A_{ev}(x') = 2\pi f_c A_s q \cdot \varphi(h, x') \quad (24)$$

which can be regarded as the balise induced voltage amplitude envelope (BIVAE) at different BTM locations.

Suppose the location of the BTM antenna is $x' = -L_g$ at time $t = 0$, and it satisfies

$$x' = vt - L_g \quad (25)$$

Substitute Equation (25) into Equation (24), and the induced voltage amplitude envelope based on train speed v takes the form

$$A_{ev}(t) = 2\pi f_c A_s q \cdot \varphi(h, vt - L_g) \quad (26)$$

Supposing that the train motion range is $x' \in [-1, 1]$ (m), train speed is $v = 300$ km/h. Based on Equation (23) and Equation (24), we simulate the change law of the balise induced voltage when the train passes by the balise, as shown in Figure 9.

In Figure 9(a), the amplitude envelop of the time-domain waveform is depicted by the dashed line, and for the convenience of analysis, we redraw it by mapping the time axis to the BTM location according to train speed, as shown in Figure 9(b).

Figure 9(b) shows that $A_{ev}(x'), x' \in [-1, 1]$ is symmetrical with respect to the center of the balise antenna, and arrives at the minimums $A_{ev}(u_1)$ and $A_{ev}(u_2)$ at u_1 and u_2, respectively, which is in accordance with the zero-value area in Figures 8(b) and 8(f). The $A_{ev}(x')$ can
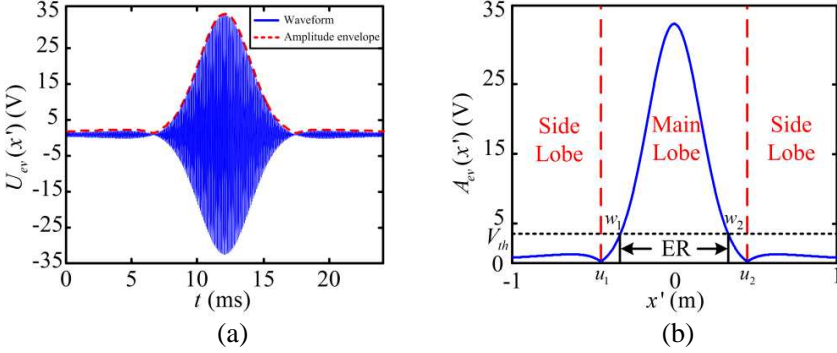
Figure 9. Simulation results of the balise induced voltage. (a) Waveform and the amplitude envelop of the balise induced voltage based on train running time. (b) Amplitude envelope of the balise induced voltage based on the BTM location, i.e., the BIVAE.

be divided into three parts, i.e., the main lobe $A_{ev}(x')$, $x' \in [u_1, u_2]$, and the two side lobes $A_{ev}(x')$, $x' \in [-1, u_1]$ and $A_{ev}(x')$, $x' \in [u_2, 1]$. Because $A_{ev}(x')$, $x' \in [-1, u_1]$, $x' \in [u_2, 1]$ is below the threshold V_{th}, the balise will remain dormant in the two side lobes, whereas in the main lobe, since the BTM is very close to the balise, the $A_{ev}(x')$ has exceeded the threshold V_{th} in the range $x' \in [w_1, w_2]$ and the balise will enter the operation state.

Generally, the point w_1 is termed the start-operation point, w_2 termed the end-operation point, the range $x' \in [w_1, w_2]$ termed the balise effective range (ER), which is calculated by

$$R = \max \left(x' | A_{ev}(x') \geq V_{th} \right) - \min \left(x' | A_{ev}(x') \geq V_{th} \right) \qquad (27)$$

According to the equation above, the ER value of the BIVAE in Figure 9(b) is $R_{ex} = 0.676$ m.

3. PERFORMANCE OPTIMIZATION OF BITS

With references to the specification of CTCS Level 1~4, we set the train speed as $v = 120$ km/h, 160 km/h, 250 km/h, and 350 km/h, respectively, and simulate the BIVAEs under different speed conditions according to Equation (26). Because the dimension of the balise antenna is relatively small, the train speed can be considered as constant within the ER.

Figure 10 shows that as train speed increases, the duration time of the train's passing by the balise decreases, causing the shape of
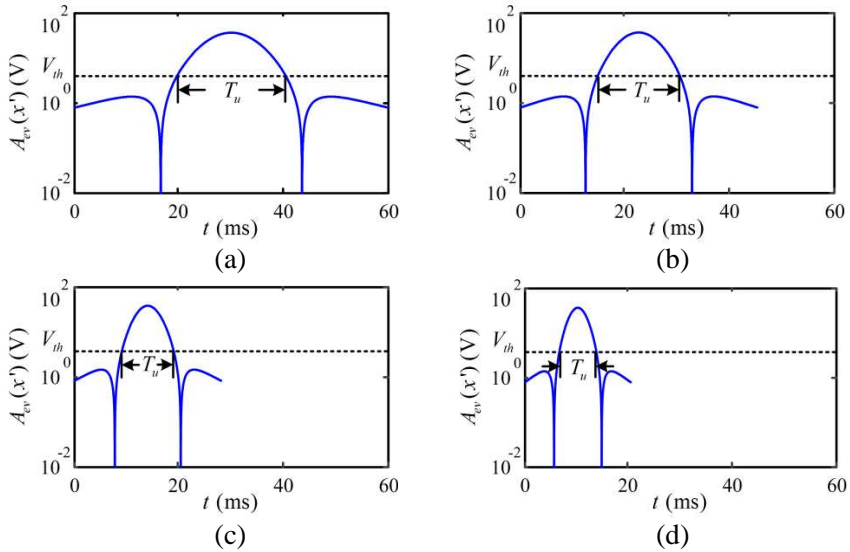
Figure 10. BIVAEs under different train speed conditions. (a) $v = 120 \, \text{km/h}$. (b) $v = 160 \, \text{km/h}$. (c) $v = 250 \, \text{km/h}$. (d) $v = 350 \, \text{km/h}$.

curve BIVAE to compress in time axis, and accordingly, decreasing the operation time T_u of the balise.

The data amount M of the telegram signal received by the BTM are given by

$$M = r_u \cdot T_u \tag{28}$$

where $r_u = 564.48 \, \text{kbit/s}$ is the up-link data transmission rate, and T_u is expressed as

$$T_u = R/v \tag{29}$$

Hereby we calculate the BTM received data amount and the corresponding telegram frames (suppose one telegram frame consists of 1023 bits) according to the two equations above, as listed in Table 2.

From Table 2 we see that the speed increase finally results in the reduction of the BTM received telegram frames, and when the speed

Table 2. BTM received data amount under different speed conditions.

Train speed (km/h)	120	160	250	350	448
Balise operation time (ms)	20.3	15.2	9.7	7.0	5.4
BTM received data amount (bits)	11448	8586	5495	3925	3069
BTM received telegram frames	11.2	8.4	5.4	3.8	3.0

reaches $350\,\mathrm{km/h}$, the complete telegram frames received are only 3. Therefore, the original security mechanism for BTM decoding which is "selecting 4 from 5" has to be adjusted to "selecting 2 from 3", which has reached the lowest requirement that ensures the normal operation of BITS. Further, we calculate the critical train speed when the complete telegram frames received by the BTM is just 3, i.e., the maximum admissible speed for the reliable operation of BITS, and the result is only $448\,\mathrm{km/h}$. From this we can see that, to meet the requirements of further speed increase, it is necessary to perform certain optimizations to the existing system to increase the BTM received data amount as well as the critical train speed.

From the working principle of BITS, we can deduce that the aim of the system performance optimization is essentially to maximize the BTM received telegram data amount, according to Equation (28) and Equation (29) and can be expressed as

$$M_{\max} = \max(r_u T_u) = r_u \cdot \max(T_u) = r_u \cdot \max(R/v) \qquad (30)$$

Equation (30) reveals that the up-link signal transmission is related to the tele-powering signal transmission, and the BTM received telegram data amount is determined by the ER value when train speed is assumed. Therefore, the performance optimization of the system is transformed to the maximization of the ER value.

Given that the balise can be mounted transversally or longitudinally, i.e., when the EF side of the balise is parallel or vertical to the OX axis. Based on the simulation conditions in Figure 9(b), we simulate the BIVAEs $A_{tr}(x')$ and $A_{ld}(x')$ when the balise is mounted transversally and longitudinally, respectively, and calculate the corresponding ER values R_{tr} and R_{ld} according to Equation (27), as shown in Figure 11.

Figure 11 shows that under the same train speed conditions, the balise operation time of the longitudinal mounting is longer than that of the transversal mounting, satisfying $R_{ld} > R_{tr}$, whereas the peak value of the transversal mounting is higher, i.e., $A_{tr}(0) > A_{ld}(0)$, indicating that the associated anti-interference ability is stronger than that of the longitudinal mounting.

Besides, from Figure 9(b) we can see that the ER value is directly related to the shape of curve $A_{ev}(x')$, while $A_{ev}(x')$ is determined by the BMH as expressed in Equation (24). According to the structures of the locomotive, track, and roadbed, and the balise mounting specifications, the range of BMH is determined as $h \in [0.26\,\mathrm{m}, 1\,\mathrm{m}]$. Then, based on the simulation conditions in Figure 9(b) and longitudinal mounting, we simulate the $A_{ev}(x')$ under different BMHs of $0.26\,\mathrm{m}$, $0.35\,\mathrm{m}$, $0.5\,\mathrm{m}$, and $0.8\,\mathrm{m}$, respectively, as shown in Figure 12.
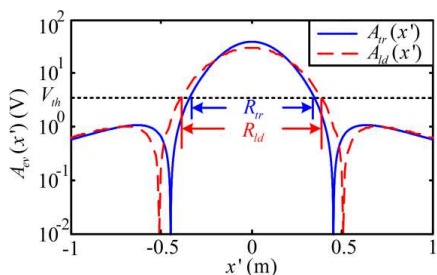
Figure 11. BIVAEs with transversal and longitudinal mounting of the balise.
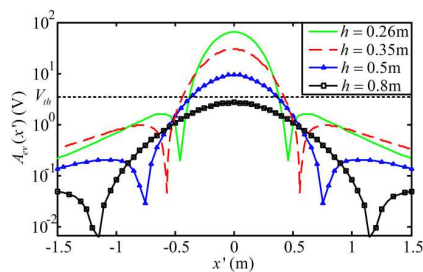
Figure 12. BIVAEs under different BMHs.

Figure 12 shows that the BMH greatly affects curve $A_{ev}(x')$. When $h > 0.8\,\text{m}$, the peak of $A_{ev}(x')$ satisfies

$$A_{ev}(0) < V_{th} \tag{31}$$

That is, the balise will not start to work under this condition. If we lower the BMH, it satisfies

$$R(h = 0.35) = \max(R(h = 0.26), R(h = 0.35), R(h = 0.5)) \tag{32}$$

Equation (32) implies that there exists an optimum value for the ER within $h \in [0.26, 0.5]$. Hereby, based on the longitudinally mounting and according to Equation (24) and Equation (27), we calculate the ER value for each BMH varying from $0.26\,\text{m}$ to $0.5\,\text{m}$ with the step of $0.001\,\text{m}$ and the results are shown in Figure 13.

Figure 13 shows that the ER value is a unimodal function of BMH, and the optimum ER value is $R_{ld}^* = 0.793\,\text{m}$ at the BMH of $h_{ld}^* = 0.381\,\text{m}$. If we still adopt the transversal mounting style, the optimum result is obtained similarly as: $R_{tr}^* = 0.713\,\text{m}$, $h_{tr}^* = 0.403\,\text{m}$.
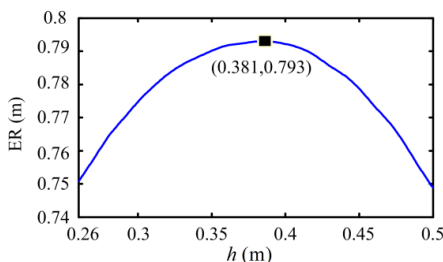
Figure 13. Optimization of the ER value based on the BMH.

4. EXPERIMENTAL VERIFICATION

To verify the proposed optimization scheme, we will have to change the balise mounting style and adjust the BMH, which is inconvenient in practice. Thus, we perform the verification under lab conditions, and the test plan is illustrated in Figure 14.
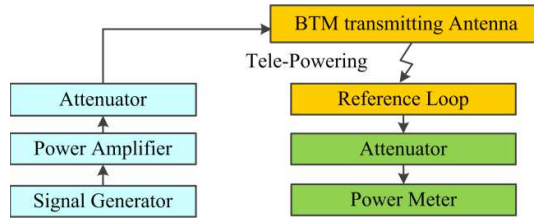
Figure 14. Test plan for the verification of the RLIVAE.

The tele-powering signal is generated by the signal generator, and through the power amplifier, the attenuator, to the BTM transmitting antenna to be radiated. To test the induced voltage signal, for convenience, we refer to the test specification [31] and use the special reference loop instead of the balise. We measure the induced voltage of the reference loop using the power meter at each BTM location in the motion range to form the reference loop induced voltage amplitude envelope (RLIVAE) which is represented by the dashed line in Figure 15, while the corresponding theoretical results are represented by the solid line.

Figure 15 shows that the measured results well agree with the theoretical ones, proving the correctness of the dynamic transmission model of the tele-powering signal built in this paper.

Further, we substitute the balise for the reference loop and add the
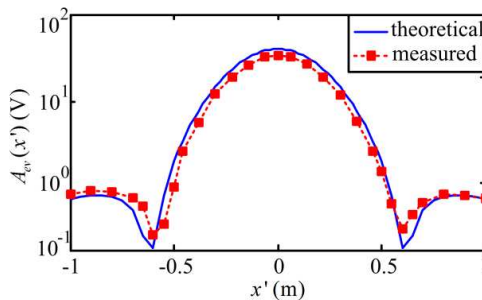
Figure 15. Measured and theoretical results of the RLIVAE.

BTM telegram decoding device to verify the validity of the proposed optimization scheme as shown in Figure 16.
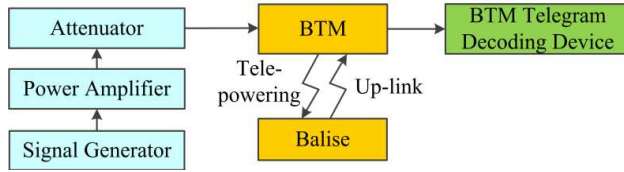
Figure 16. Test plan for verification of the optimization scheme.

Under the conditions when the balise is mounted transversally and longitudinally, respectively, we measure the start-operation position and the end-operation position of the balise when the BMH is $h = 0.26\,\text{m}$, $0.30\,\text{m}$, $0.33\,\text{m}$, $0.37\,\text{m}$, $0.42\,\text{m}$, $0.5\,\text{m}$, etc., and calculate the ER values according to Equation (27), the results are represented by the dashed lines in Figures 17(a) and 17(b), respectively. Meanwhile, based on the same testing conditions, the corresponding theoretical results are obtained and represented by the solid lines in Figures 17(a) and 17(b), respectively. Considering measurement accuracy, the measured results are given in two significant figures.

Figure 17 shows that the measured results are very close to the corresponding theoretical ones, and the variation tendency is consistent with the theoretical one in Figure 13. If we maintain the balise mounting as transversal, the ER value for the existing system is $R_{ex}^* = 0.67\,\text{m}$ when $h_{ex}^* = 0.33\,\text{m}$, whereas the optimum ER value is $R_{trM}^* = 0.71\,\text{m}$ when $h_{trM}^* = 0.40\,\text{m}$, showing a slight increase, also
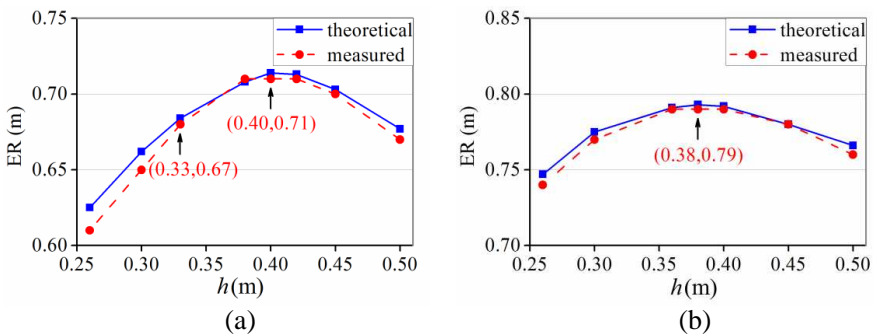
Figure 17. Verification of the optimization results under different balise mounting styles. (a) Transversal mounting. (b) Longitudinal mounting.

indicating that the BTM of the existing system isn't mounted at the best position. If the balise is mounted longitudinally, the optimum ER value is $R^*_{ldM} = 0.79\,\text{m}$ when $h^*_{ldM} = 0.38\,\text{m}$, exhibiting a great promotion over the existing one.

Based on the measured optimum results, we calculate the BTM received data amount and telegram frames under different train speed conditions according to Equations (28) and (29) when the balise is mounted transversally and longitudinally, respectively, as listed in Table 3 and Table 4.

Table 3. BTM received data amount under different speed conditions with the balise mounted transversally.

Train speed (km/h)	120	160	250	350	470
Balise operation time (ms)	21.3	16.0	10.2	7.3	5.4
BTM received data amount (bits)	12023	9018	5771	4122	3069
BTM received telegram frames	11.8	8.8	5.6	4.0	3.0

Table 4. BTM received data amount under different speed conditions with the balise mounted longitudinally.

Train speed (km/h)	120	160	250	350	523
Balise operation time (ms)	23.7	17.8	11.4	8.1	5.4
BTM received data amount (bits)	13378	10034	6422	4587	3069
BTM received telegram frames	13.1	9.8	6.3	4.5	3.0

Compared with the results of the existing system as listed in Table 2, the BTM received data amount and the telegram frames have increased a lot after optimization. Considering the critical decoding frame condition, the critical train speeds are 470 km/h for transversal mounting and 523 km/h for longitudinal mounting, showing big promotions over the 448 km/h of the existing one.

5. DISCUSSIONS

The performance optimization based on the tele-powering signal transmission described above is mainly from perspectives of the balise mounting style and the BMH, yet Equation (12) shows that the transmission process is also affected by the pitch angle of the BTM antenna α. Thereby, we discuss the system optimization with respect to the BTM pitch angle.

In Equation (12), if we do not let $\alpha = 0$, through similar derivations, Equation (24) can be rewritten as

$$A_{ev}(x') = 2\pi f_c A_s q\varphi(\alpha, h, x') \tag{33}$$

Based on the simulation conditions in Figure 9(b), we let α be $0°$, $30°$, $45°$, $60°$, $90°$, respectively, and simulate the corresponding BIVAEs according to Equation (33) as shown in Figure 18.

Figure 18 shows that as the pitch angle increases from $0°$ to $90°$, the peak value of the $A_{ev}(x')$ gradually decreases, and the shape of curve $A_{ev}(x')$ changes from unimodal symmetrical to bimodal asymmetrical and then to bimodal symmetrical. To be specific, when $\alpha = 0$ as shown in Figure 18(a), curve $A_{ev}(x')$ has three parts, one main lobe whose peak value is very high and two side lobes whose peak values are quite low. When the pitch angle continues to increase as shown in Figures 18(b)–18(d), the peak value of the main lobe gradually decreases, and the left side lobe nearly disappears, whereas the right side lobe gradually uplifts, making its peak value exceed the threshold V_{th} and activate the balise. When the pitch angle reaches $\alpha = 90°$ as shown in Figure 18(e), the $A_{ev}(x')$ is a bimodal symmetrical curve without the difference of main lobe or side lobe, and the two lobes have an equivalent balise effective range marked as ER_1 and ER_2. Between
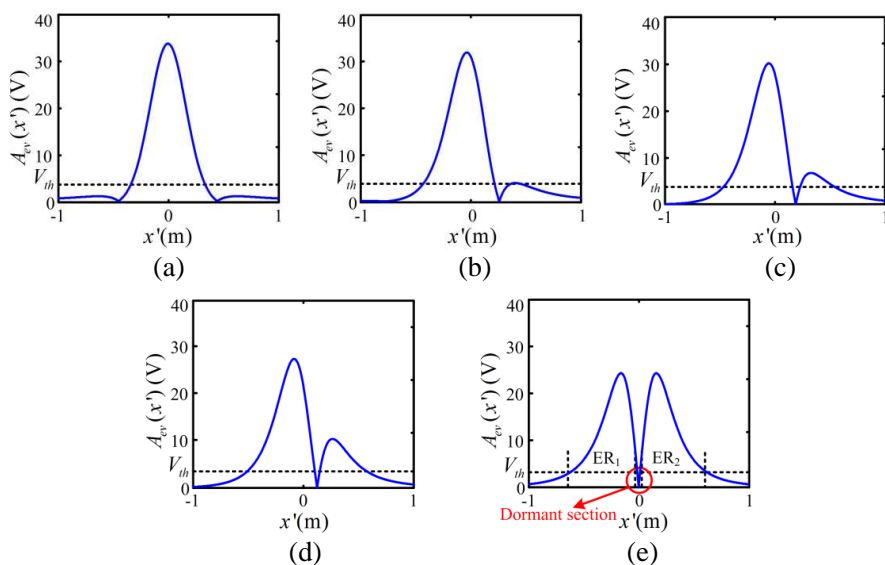
Figure 18. BIVAEs under different BTM pitch angle conditions. (a) $\alpha = 0$. (b) $\alpha = 30°$. (c) $\alpha = 45°$. (d) $\alpha = 60°$. (e) $\alpha = 90°$.

the two lobes there is a small section called the dormant section where the $A_{ev}(x')$ is below V_{th}, thus the ER value of the system satisfies

$$\mathrm{ER} = \mathrm{ER}_1 = \mathrm{ER}_2 \tag{34}$$

Hereby we propose a potential optimization scheme: if we could change the internal circuit of the balise or improve the BTM decoding mechanism, enabling it to automatically ignore the dormant section and continue transmitting the up-link signal, then the ER value of the system can be further increased and satisfy

$$\mathrm{ER} = \mathrm{ER}_1 + \mathrm{ER}_2 \tag{35}$$

Based on the test plan in Figure 16 and the transversal mounting of the balise, we measure the ER values according to Equation (35) under different pitch angle conditions of $\alpha = 30°$, $45°$, $60°$, and $90°$, respectively when the BMH is $h = 0.26\,\mathrm{m}$, $0.30\,\mathrm{m}$, $0.33\,\mathrm{m}$, $0.37\,\mathrm{m}$, $0.49\,\mathrm{m}$ and $0.62\,\mathrm{m}$, etc., the measured and the corresponding
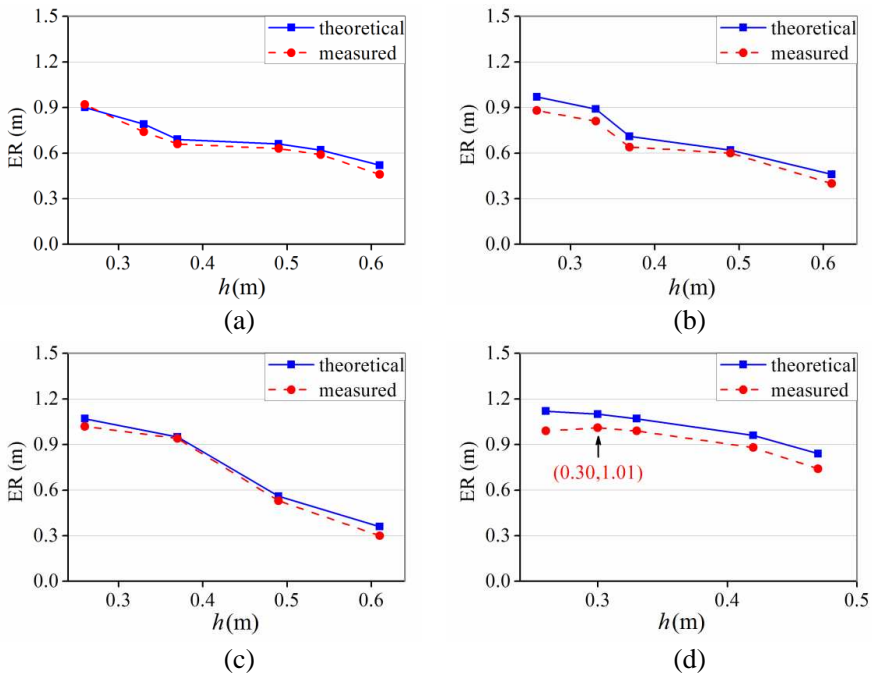
Figure 19. Measured and theoretical ER values under different BTM pitch angle and height conditions. (a) $\alpha = 30°$. (b) $\alpha = 45°$. (c) $\alpha = 60°$. (d) $\alpha = 90°$.

theoretical results are represented by the dashed and solid lines in Figure 19, respectively.

Figure 19 shows that the variation tendency of the measured results is consistent with that of the theoretical ones, and the ER value increases monotonically as the BMH decreases. When $\alpha = 90°$ (vertical mounting of the BTM antenna) and $h = 0.30\,\text{m}$, the measured ER value has reached $R_\alpha = 1.01\,\text{m}$, and the corresponding critical speed is $669\,\text{km/h}$, which is much higher than the existing $448\,\text{km/h}$ and also higher than the optimized $523\,\text{km/h}$.

6. CONCLUSION

In this paper, the dynamic transmission process of the balise tele-powering signal is modeled using finite element method, and it is proved that the simplified model has sufficient accuracy for presenting the desired characteristics. Then, the transmission process is studied using electromagnetic field theory, and the expression of balise induced voltage is derived. From simulation analysis, the change law of the BIVAE based on train location and train speed is obtained, and ER is recommended to be the evaluation criterion of the system performance. To meet the requirements for the further increase of train speed, the performance optimization is implemented from two perspectives of the balise mounting style and the BMH, and the corresponding optimum ER values are obtained.

This paper provides two optimization schemes that have been proved experimentally: if the balise is mounted transversally, the optimum ER value is $0.71\,\text{m}$ at the BMH of $0.40\,\text{m}$ with the critical speed of $470\,\text{km/h}$. If the balise is mounted longitudinally, the optimum ER value is $0.79\,\text{m}$ at the BMH of $0.38\,\text{m}$ with the critical speed of $523\,\text{km/h}$, demonstrating big increase over the existing $448\,\text{km/h}$ and making the system adaptable to higher train operation speed. In addition, the influence law of the BTM pitch angle on ER is discussed, and we find that, if the internal circuits of the balise or the BTM decoding mechanism are improved, then based on the vertical mounting of the BTM antenna, the system performance will have huge promotion with the critical speed up to $669\,\text{km/h}$.

ACKNOWLEDGMENT

REFERENCES

1. http://europe.chinadaily.com.cn/video/2010-12/03/content_116-50575.htm.

2. China Ministry of Railway, "Principles of application for the balise in CTCS level 2 (V1.0)," 2008.

3. Moshe, G., "Development and impact of the modern high-speed train: A review," *Transport Reviews*, Vol. 26, No. 5, 593–611, 2006.

4. Pu, S., J.-H. Wang, and Z. Zhang, "Estimation for small-scale fading characteristics of RF wireless link under railway communication environment using integrative modeling technique," *Progress In Electromagnetics Research*, Vol. 106, 395–417, 2010.

5. Zhao, L.-H. and W.-S. Shi, "Induction coupling between jointless track circuits and track-circuit-reader antenna," *Progress In Electromagnetics Research*, Vol. 138, 173–196, 2013.

6. Xiao, T. and H.-B. Zhao, "Safety research of the coding strategy of eurobalise," *Journal of China Railway Society*, Vol. 30, No. 6, 127–130, 2008.

7. Zhao, L.-H., Z.-K. Li, and W.-N. Liu, "An integrated uplink-signal detection method of railway balise system based on wavelet ridge," *3rd IEEE International Symposium on Microwave, Antenna, Propagation and EMC Technologies*, 78–83, 2009.

8. Xu, N., J.-L. Zhang, and C.-J. Wang, "Key technologies of the balise on-board test equipment under high-speed conditions," *China Railway Science*, Vol. 31, No. 4, 131–137, 2010.

9. Zeng, J.-Y. and H.-B. Zhao, "Research of the balise transmission module test system," *Journal of Beijing Jiaotong University*, Vol. 32, No. 2, 80–83, 2008.

10. Sharma, R. and R.-M. Lourde, "Crosstalk reduction in balise and infill loops in automatic train control," *11th INES*, 39–44, Budapest, Hungary, 2007.

11. Sevillano, J.-F., J. Mendizabal, and I. Sancho, "Reliability analysis of an ERTMS on-board balise transmission equipment," *Reliability, Risk and Safety: Theory and Applications*, Vol. 1, No. 3, 2317–2324, 2010.

12. Dhahbi, S. and T. Abbas, "Study of the high-speed trains positioning system: European signaling system ERTMS/ETCS," *4th International Conference on Logistics*, 468–473, 2011.

13. Sandidzadeh, M. and A. Khodadadi, "Optimization of balise placement in a railway track using a vehicle, an odometer and

genetic algorithm," *Journal of Scientific* & *Industrial Research*, Vol. 70, No. 3, 210–214, 2011.

14. Zhao, L.-H. and Y. Jiang, "Modeling and simulation of balise uplink data transmission based on finite element method," *Journal of Theoretical and Applied Information Technology*, Vol. 46, No. 2, 867–874, 2012.

15. Wei, H.-Y. and M. Soleimani, "Two-phase low conductivity flow imaging using magnetic induction tomography," *Progress In Electromagnetics Research*, Vol.131, 99–115, 2012.

16. Cabanas, M.-F., F. Pedrayes, M. G. Melero, C. H. Rojas, G. A. Orcajo, J. M. Cano, and J. G. Norniella, "Insulation fault diagnosis in high voltage power transformers by means of leakage flux analysis," *Progress In Electromagnetics Research*, Vol. 114, 211–234, 2011.

17. Torkaman, H. and E. Afjei, "Comparison of three novel types of two-phase switched reluctance motors using finite element method," *Progress In Electromagnetics Research*, Vol. 125, 151–164, 2012.

18. Lecointe, J.-P., B. Cassoret, and J.-F. Brudny, "Distinction of toothing and saturation effects on magnetic noise of induction motors," *Progress In Electromagnetics Research*, Vol. 112, 125–137, 2011.

19. Touati, S., R. Ibtiouen, O. Touhami, et al., "Experimental investigation and optimization of permanent magnet motor based on coupling boundary element method with permeances network," *Progress In Electromagnetics Research*, Vol. 111, 71–90, 2011.

20. Zhao, W., M. Cheng, R. Cao, et al., "Experimental comparison of remedial single-channel operations for redundant flux-switching permanent-magnet motor drive," *Progress In Electromagnetics Research*, Vol. 123, 189–204, 2012.

21. Mahmoudi, A., N.-A. Rahim, and H.-W. Ping, "Axial-flux permanent-magnet motor design for electric vehicle direct drive using sizing equation and finite element analysis," *Progress In Electromagnetics Research*, Vol. 122, 467–496, 2012.

22. Cheshmehbeigi, H.-M., S.-E. Afjei, and B. Nasiri, "Electromagnetic design based on hybrid analytical and 3-D finite element method for novel two layers BLDC machine," *Progress In Electromagnetics Research*, Vol. 136, 141–155, 2013.

23. Fotyga, G., K. Nyka, and M. Mrozowski, "Efficient model order reduction for FEM analysis of waveguide structures and resonators," *Progress In Electromagnetics Research*, Vol. 127, 277–295, 2012.

24. Azpurua, M.-A., "A semi-analytical method for the design of coil-systems for homogeneous magneto-static field generation," *Progress In Electromagnetics Research B*, Vol. 37, 171–189, 2012.

25. Ravaud, R. and G. Lemarquand, "Comparison of the Coulombian and Amperian current models for calculating the magnetic field produced by radially magnetized arc-shaped permanent magnets," *Progress In Electromagnetics Research*, Vol. 95, 309–327, 2009.

26. Pelloni, S., A. Ligabue, and P. Lazzeretti, "Ring-current models from the differential Biot-Savart law," *Organic Letters*, Vol. 24, 4451–4454, 2004.

27. Lopez-Ramos, A., J.-R. Menendez, and C. Pique, "Conditions for the validity of Faraday's law of induction and their experimental confirmation," *European Journal of Physics*, Vol. 29, No. 5, 1069–1076, 2008.

28. Gustafsson, M. and S. Nordebo, "Bandwidth, Q factor, and resonance models of antennas," *Progress In Electromagnetics Research*, Vol. 62, 1–20, 2006.

29. Rezaee, P., M. Tayarani, and R. Knöchel, "Active learning method for the determination of coupling factor and external Q in microstrip filter design," *Progress In Electromagnetics Research*, Vol. 120, 459–479, 2011.

30. UNISIG SUBSET-036-v2.4.1, "FFFIS for Eurobalise," 2010.

31. UNISIG SUBSET-085-v2.2.2, "Test Specification for Eurobalise FFFIS," 2010.